

 Open access • Journal Article • DOI:10.1021/JP1016054

A Systematic Study of the Effect of Silver on the Chelation of Formic Acid to a Titanium Precursor and the Resulting Effect on the Anatase to Rutile Transformation of TiO₂

— [Source link](#) 

Nicholas T. Nolan, Michael K. Seery, Steven J. Hinder, Linda F. Healy ...+1 more authors





Institutions: Dublin Institute of Technology

Published on: 12 Jul 2010 - Journal of Physical Chemistry C (American Chemical Society)

Topics: Anatase, Rutile, Formate, Fourier transform infrared spectroscopy and Raman spectroscopy

Related papers:

- [A review on the visible light active titanium dioxide photocatalysts for environmental applications](#)
- [Visible-Light Photocatalysis in Nitrogen-Doped Titanium Oxides](#)
- [Silver Doped Titanium Dioxide Nanomaterials for Enhanced Visible Light Photocatalysis](#)
- [Electrochemical Photolysis of Water at a Semiconductor Electrode](#)
- [Oxygen Rich Titania: A Dopant Free, High Temperature Stable, and Visible-Light Active Anatase Photocatalyst](#)

Share this paper:    

View more about this paper here: <https://typeset.io/papers/a-systematic-study-of-the-effect-of-silver-on-the-chelation-1aamz8ymsj>

2010-06-24

A Systematic Study of the Effect of Silver on the Chelation of Formic Acid to a Titanium Precursor and the Resulting Effect on the Anatase to Rutile Transformation of TiO₂

Nicholas Nolan

Technological University Dublin, nicholas.nolan@tudublin.ie

Michael Seery

Technological University Dublin, michael.seery@tudublin.ie

Steve Hinder

University of Surrey, S.Hinder@surrey.ac.uk

See next page for additional authors

Follow this and additional works at: <https://arrow.tudublin.ie/cenresart>

 Part of the [Materials Chemistry Commons](#), and the [Physical Chemistry Commons](#)

Recommended Citation

Nolan, N. et al. (2010) :A Systematic Study of the Effect of Silver on the Chelation of Formic Acid to a Titanium Precursor and the Resulting Effect on the Anatase to Rutile Transformation of TiO₂. *Journal of Physical Chemistry C*, 114, 2010, pp. 13026 - 13034. doi:10.1021/jp1016054

This Article is brought to you for free and open access by the Crest: Centre for Research in Engineering Surface Technology at ARROW@TU Dublin. It has been accepted for inclusion in Articles by an authorized administrator of ARROW@TU Dublin. For more information, please contact arrow.admin@tudublin.ie, aisling.coyne@tudublin.ie.



This work is licensed under a [Creative Commons Attribution-NonCommercial-Share Alike 4.0 License](#)
Funder: Environmental Protection Agency, Ireland

Authors

Nicholas Nolan, Michael Seery, Steve Hinder, Linda Healy, and Suresh Pillai

A Systematic Study of the Effect of Silver on the Chelation of Formic Acid to a Titanium Precursor and the Resulting Effect on the Anatase to Rutile Transformation of TiO₂

Nicholas T. Nolan,^{†,‡} Michael K. Seery,^{*,†} Steven J. Hinder,[§] Linda F. Healy,[†] and Suresh C. Pillai^{*,§}

School of Chemical and Pharmaceutical Sciences, Dublin Institute of Technology, Kevin Street, Dublin 8, Ireland, Centre for Research in Engineering Surface Technology, Focas Institute, Dublin Institute of Technology, Kevin Street, Dublin 8, Ireland, and The Surface Analysis Laboratory, Faculty of Engineering and Physical Sciences, University of Surrey, GU2 7XH, United Kingdom

Received: February 23, 2010; Revised Manuscript Received: May 17, 2010

Anatase to rutile transition in an unmodified synthetic titania usually occurs at a temperature range of 600–700 °C. Various methods such as addition of metallic and nonmetallic dopants and modifying the precursor have previously been reported to influence the anatase to rutile transition temperature. In the current study, the effect of addition of increasing amounts of silver to the extent of chelation of a formate group to a titanium precursor and the resulting effects on the transformation of anatase to rutile has been studied. The addition of silver (0, 1, 3, and 5 mol %) on the anatase to rutile transformation temperature has been systematically followed by Fourier transform infrared (FTIR), Raman, X-ray diffraction (XRD), differential scanning calorimetry, and X-ray photoelectron spectroscopy (XPS) studies. From the FTIR and Raman spectroscopy studies it was observed that the incorporation of silver caused a reduction in the intensity of the COO⁻ stretches indicating that the titania formate bridging complex is becoming weaker in the presence of silver. XRD studies indicated an early rutile formation for the silver-doped samples. XRD of the samples calcined at 700 °C showed that 5 mol % Ag TiO₂ contained both anatase (46%) and rutile (54%), whereas the undoped sample primarily consists of anatase (95%). At 800 °C all silver doped samples converted to 100% rutile and the undoped TiO₂ consisted of both anatase (55%) and rutile (45%). XPS analysis showed that Ag⁰ and Ag₂O has been formed on the surface of the titania formate complex without calcination (>100 °C) indicating that photo-oxidation has occurred. FTIR, Raman, and XPS studies confirmed that the presence of silver in the xerogel before calcination may be responsible for the reduction of the titanium formate bridge. It was concluded that the presence of silver (Ag₂O and Ag⁰) hindered bridging ligands, which resulted in a weakened titanium gel network. This structurally weakened gel network could easily be collapsed during calcination, and it favors an early rutile formation.

Introduction

Titanium dioxide semiconductor photocatalysis has attracted the attention of several researchers in the past decade due to its environmental applications such as air purification and water remediation.^{1–10} Anatase, rutile, and brookite are the three polymorphs of TiO₂ and differ only in arrangement of their [TiO₆]²⁻ octahedra; anatase (tetragonal) consists of octahedrals sharing vertices; rutile (tetragonal) is connected by edges, and in brookite (orthorhombic) both edges and vertices are connected.^{11–13} Rutile is found freely in nature, but all three can be synthetically prepared. Rutile is the thermodynamically stable phase, while anatase and brookite are both metastable, transferring to rutile under heat treatment at temperatures typically ranging between 600–700 °C.¹¹ Anatase is widely regarded as the most photocatalytically active of the three crystalline structures.^{13–15} Titanium dioxide is the most widely investigated photocatalyst because of its ease of preparation, availability, strong oxidizing power, nontoxicity, and long-term

stability.^{7,16} However, because of its large band gap (3.2 eV for anatase), TiO₂ can only be activated upon irradiation with a photon of light <390 nm, limiting its use under solar irradiation.^{16–18} Because of this, researchers have been focusing their attention on ways to improve the photocatalytic efficiency of TiO₂ under irradiation with visible light (>400 nm).

Asahi et al. have reported nitrogen doped TiO₂ promoting photocatalytic activity up to $\lambda = 520$ nm claiming that the presence of nitrogen narrows the band gap of TiO₂ thus making it capable of performing visible light driven photocatalysis.¹⁹ However, Ihara et al. suggested that it is the oxygen vacancies that contributed to the visible light activity, and the doped nitrogen only enhanced the stabilization of these oxygen vacancies.²⁰ They also confirmed this role of oxygen vacancies in plasma-treated TiO₂ photocatalysts.²⁰ In addition the structural oxygen vacancies causing visible light photocatalytic activity was also reported by Martyanov et al.²¹ Further studies with nonmetal dopants, S,²² C,²³ I,²⁴ Br, and Cl,¹⁸ also show red shifts in band gap edge of TiO₂.

Transition metal doping has also given promising results for visible light activated TiO₂ by extending the absorption spectra into the visible region. Much research has focused on the transition metal ion Fe³⁺^{25–29} whereby its incorporation into the crystal lattice results in the formation of new energy levels

* To whom correspondence should be addressed. E-mail: michael.seery@dit.ie (M.K.S.); suresh.pillai@dit.ie (S.C.P.).

[†] School of Chemical and Pharmaceutical Sciences, Dublin Institute of Technology.

[‡] CREST, Dublin Institute of Technology.

[§] School of Engineering, University of Surrey.

72 between the valence band and the conduction band.³⁰ Deposition
73 of noble metals Ag, Au, Pt, and Pd on the surface of TiO₂
74 enhance the photocatalytic efficiency by acting as an electron
75 trap, promoting interfacial charge transfer and therefore delaying
76 recombination of the electron-hole pair.^{27,31–34}

77 Many researchers have focused on modifying TiO₂ with Ag.
78 For example, Chao et al. reported the effect of Ag doping on
79 the phase transformation and grain growth of sol-gel TiO₂
80 powder.³⁵ Kuo et al. showed through X-ray diffraction (XRD)
81 and X-ray photoelectron spectroscopy (XPS) that silver on TiO₂
82 surface coatings was easily oxidized into silver oxide (Ag₂O)
83 and that the addition of silver causes a reduction in photolu-
84 minescence (PL) intensity as found by PL spectroscopy.³⁶ This
85 group previously showed enhanced visible light photocatalysis
86 with Ag modified TiO₂.³⁷ Choi et al. controlled the ratio of
87 anatase and rutile phases through the addition of surfactants.³⁸
88 The effect of precursor chelation on anatase to rutile transition
89 has also been reported previously. Acetic acid,³⁹ formic acid,⁴⁰
90 urea,⁴¹ sulfuric acid,⁴² and ammonium sulfate⁴³ have previously
91 been employed to study the effect of a chelating agent on the
92 anatase to rutile transformation in the TiO₂ photocatalyst.
93 However, there are no systematic studies on the effect of silver
94 doping on chelation and anatase to rutile transformation.

95 The current paper reports a systematic study on how the
96 addition of increasing amounts of silver affects the extent of
97 chelation of a formate group to a titanium precursor and how
98 the resulting reduction in formate chelation causes early
99 transformation of anatase to rutile. The effect of the addition
100 of silver on structural changes is investigated by characterizing
101 the sample in its amorphous state (i.e., before it is calcined)
102 with XPS, IR, and Raman studies. XRD was used to determine
103 the crystalline phase of the calcined samples, and differential
104 scanning calorimetry (DSC) was employed to examine the
105 thermal events of the sample through heat treatment. The effect
106 of silver on the electronic transitions of crystalline TiO₂ is shown
107 through UV-vis and PL spectroscopy. To the best of the
108 authors' knowledge this is the first paper to report the effect of
109 silver on a titanium formate complex before calcination and
110 the subsequent effects of the presence of silver upon calcination.

111 Experimental Section

112 Titanium tetraisopropoxide (TTIP)(97%), formic acid (98%),
113 and silver nitrate (99%) were purchased from Aldrich and used
114 without further purification. Deionized water was used in all
115 experimental preparations. The samples were prepared by a
116 modified sol-gel route.⁴⁰ Titanium tetraisopropoxide (36 mL)
117 was added to formic acid (19 mL) under stirring. Water (9 mL)
118 was added, and a thick paste was formed. The TTIP, formic
119 acid, and water were used in 1:4:4 molar ratios. The mixture
120 was stirred for 2 h and filtered, and the filtrate was dried in an
121 oven at 100 °C for 12 h. To prepare silver doped titania, the
122 above procedure was repeated, including silver nitrate (1, 3,
123 and 5 mol %) in the water before it was added to the TTIP/
124 formic acid mixture. The dried powders were calcined at 300,
125 500, 700, and 900 °C for 2 h at a ramp rate of 3 °C/min. A
126 Siemens D 500 X-ray diffractometer, with a diffraction angle
127 range 2 Θ = 20–80° using Cu K α radiation, was used to collect
128 XRD diffractograms. The mass fraction of rutile (X_R) in the
129 calcined samples was calculated using the Spurr equation⁴⁴ (eq
130 1)

$$X_R = \frac{1}{1 + 0.8(I_A/I_R)} \quad (1)$$

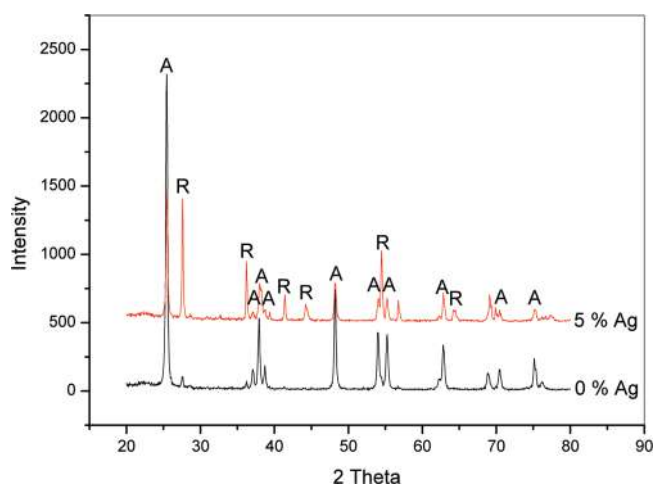


Figure 1. XRD of 0 and 5% Ag TiO₂ powders calcined at 700 °C.

where I_A is the main intensity of anatase (101) peak and I_R is
the main intensity of rutile (110) peak.

The crystallite size (T) was estimated using the Scherrer
equation³⁷ (eq 2)

$$T = \frac{0.9\lambda}{\beta \cos \theta} \quad (2)$$

where T is the crystalline size, λ is the X-ray wavelength, θ is
the Bragg angle, and β is the line broadening.

A Perkin-Elmer Lambda 900 UV-vis absorption spectro-
photometer was used to record absorption and diffuse reflectance
spectra; samples were mixed in KBr (1:20 sample KBr) and
pressed into a tablet; a KBr tablet made under the same
conditions was used as a reference. IR spectra were obtained
using a Perkin-Elmer GX FTIR spectrometer and recorded as a
KBr disk (1:10 sample/KBr); Raman spectra were recorded on
an ISA Labram, employing an argon laser (514.5 nm) as an
excitation source. PL was recorded on a Perkin-Elmer LS55
luminescence spectrometer using an excitation wavelength of
320 nm. Approximately 5 mg of sample was placed into an
aluminum sample pan for DSC using an empty aluminum pan
as a reference. All DSC were recorded on a Shimadzu DSC-60
between 25 and 600 °C at a ramp rate of 20 °C/min.

151 Results and Discussion

XRD. XRD was carried out on the calcined samples in order
to determine the crystalline phase of the samples. All samples
calcined at 300 °C were amorphous. Crystalline anatase TiO₂
was present for all samples calcined at 500 and 600 °C.
However, at 700 °C the diffractogram (Figure 1) showed that 5
mol % Ag TiO₂ contained both anatase (46%) and rutile (54%),
but TiO₂ without silver consisted mainly of anatase (95%). This
indicated that the presence of increased amounts of silver
promotes the anatase to rutile transformation.

Promotion of phase transformation by the addition of silver
is believed to be caused by the following factors.³⁵ Decreasing
anatase grain size (Figure 2) results in an increase in the total
boundary energy for the TiO₂ powder. The driving force for
rutile grain growth is therefore increased, which promotes
anatase to rutile phase transformation.⁴⁵ As the transformation
of anatase to rutile is a mechanism of nucleation and growth,^{46,47}
an increased amount of nucleation sites would favor rutile
formation. Phase transformation is also governed by such effects
as defect concentration⁴⁸ and grain boundary concentration,⁴⁹

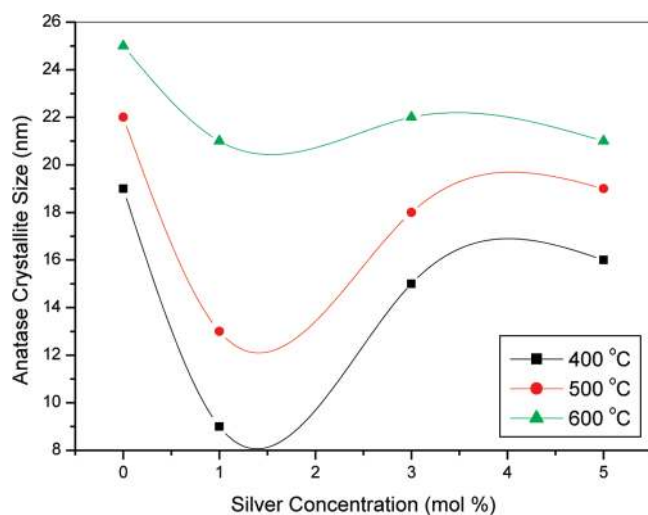
Anatase to Rutile Transformation of TiO₂

Figure 2. Variation in the nanocrystallite size (from XRD) as a function of increase in concentration of silver, at different calcination temperatures.

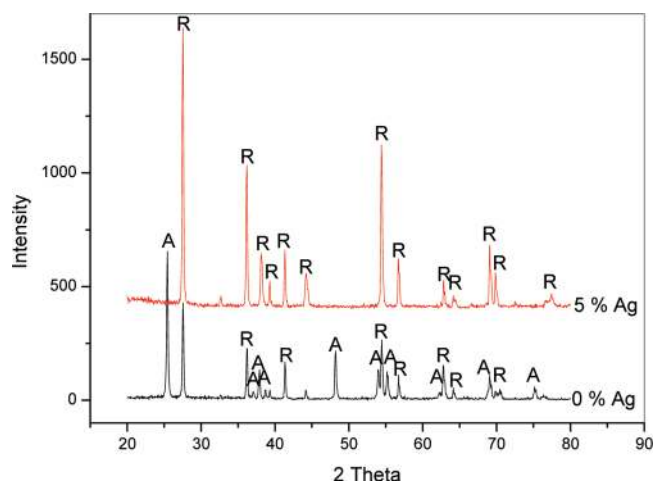


Figure 3. XRD of 0 and 5% Ag TiO₂ powders calcined at 800 °C.

171 the presence of which can be expected to be increased with
 172 greater surface areas. Rutile nucleation is thus enhanced as the
 173 presence of defect sites is increased. Therefore, an increase in
 174 the number of defect sites promotes anatase to rutile transforma-
 175 tion at lower temperatures.³⁵

176 At 800 °C, the undoped TiO₂ sample consisted of both anatase
 177 (55%) and rutile (45%), whereas the silver-doped samples were
 178 all 100% rutile (Figure 3). A higher Ag concentration promotes
 179 earlier phase transformation. Figures 1 and 3 show that the
 180 presence of silver promotes the formation of rutile.³⁵

181 The radius of Ag⁺ ion (126 pm) is much larger than that of
 182 the Ti⁴⁺ ion (68 pm) and so Ag⁺ ions cannot enter the lattice
 183 of anatase TiO₂.^{35,37} However, migration of the Ag⁺ ions from
 184 bulk anatase grains to the anatase grain surface can occur during
 185 calcination.^{35,37} With Ag migrating to the TiO₂ surface, surface
 186 defects in the anatase grains will increase. This results in a
 187 greater number of nucleation sites for the formation of rutile,
 188 again, promoting phase transformation. Oxygen vacancies may
 189 also influence the anatase to rutile transformation.^{35,50,51} Previous
 190 reports^{50,51} indicate that the concentration of oxygen vacancies
 191 at the surface of anatase increases with Ag doping. This favors
 192 the ionic rearrangement necessary for the structure changes
 193 associated with rutile phase formation.³⁵

194 An alternate effect that the silver may have on early rutile
 195 formation is that Ag cations may be easily reduced. The reduced

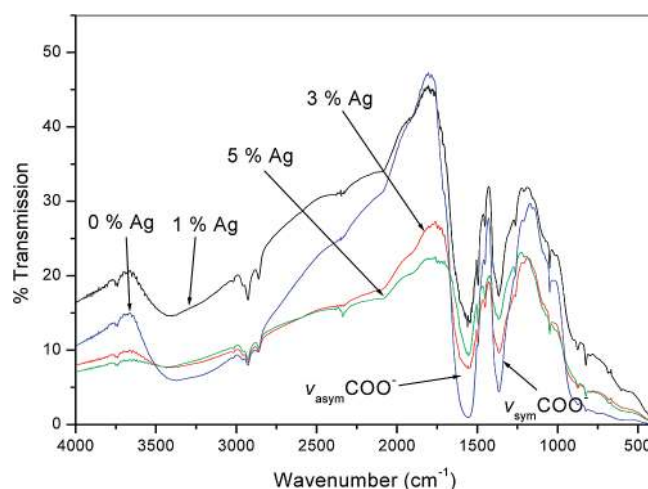


Figure 4. IR spectra of TiO₂ powders with different mol % silver content after aging at 100 °C.

196 Ag⁺ ions can spread on the anatase surface to Ag⁰ by heat. Photo
 197 reduction of the Ag⁺ ions may also occur as the samples were
 198 never protected from light irradiation.^{52,53} Oxygen vacancies will
 199 occur for charge compensation caused by Ag⁺ reduction, and
 200 again these oxygen vacancies are favored for the formation of
 201 rutile.^{35,50,51} To further investigate the role silver plays in altering
 202 the transformation temperature of TiO₂ in this study, it is
 203 necessary to understand the structure of the oligomer before
 204 calcination. To gain insight on this, DSC, IR, Raman, and XPS
 205 were carried out on the powders before calcination.

IR Spectroscopy. The influence of silver on the structure of
 206 the TiO powders was investigated before calcination using IR
 207 and Raman spectroscopy. Figure 4 shows IR spectra of the
 208 doped and undoped powders. Symmetric and asymmetric COO⁻
 209 stretches at ~1360 and 1540 cm⁻¹, respectively, indicated that
 210 the formic acid forms a bidentate bridge with the titanium
 211 precursor.^{40,54-56}

212 Figure 4 also shows that silver clearly reduces the intensity
 213 of the COO⁻ stretches as with each increase in Ag concentration
 214 there is a reduction in intensity of both the asymmetric and
 215 symmetric COO⁻ peaks. This result provides evidence for an
 216 alternative mechanism to those stated above for early anatase
 217 to rutile transformation in the presence of silver. In fact, silver
 218 may influence the anatase to rutile transformation through
 219 interactions with the titanium precursor in the early stages of
 220 the sol-gel synthesis. These interactions may ultimately alter
 221 the condensation pathway, resulting in a weakened TiO₂
 222 oligomer network.

223 To compare the effects of aging at 100 °C, IR spectra of
 224 samples 0 and 5 mol % silver TiO₂ were recorded before and
 225 after aging (Figures 5 and 6).

226 After both samples are aged at 100 °C for 12 h there is a
 227 significant reduction in the bridging formate COO⁻ stretches
 228 of the 5% silver doped sample, whereas the TiO₂ sample without
 229 silver does not show a significant reduction in the carboxylate
 230 stretches. Since the boiling point of formic acid is 101 °C, it is
 231 possible that the formic acid is displaced by the presence of
 232 silver and is then evaporated upon aging.

Raman Spectroscopy. Raman spectroscopy analysis was
 234 carried out on the powders before they were calcined to support
 235 IR spectroscopy results.

236 The Raman spectra of the doped and undoped TiO₂ samples,
 237 (Figure 7) supports the IR results. As the silver content is
 238 increased, the asymmetric and symmetric COO⁻ stretches (1570
 239 and 1390 cm⁻¹) decrease accordingly. The addition of silver
 240

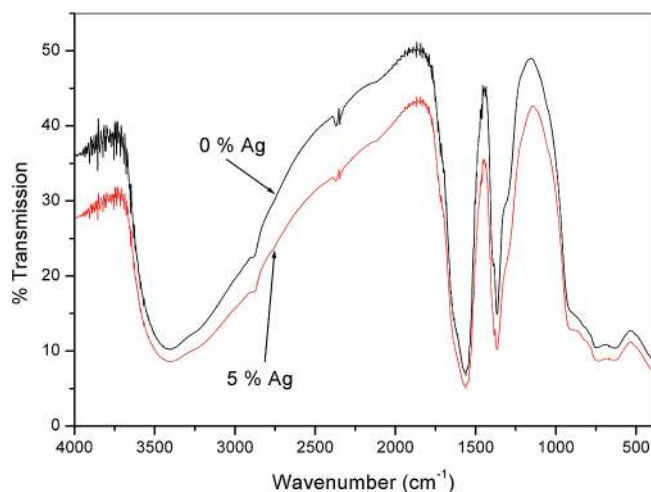


Figure 5. IR spectra of TiO₂ powders with different mol % silver content before aging.

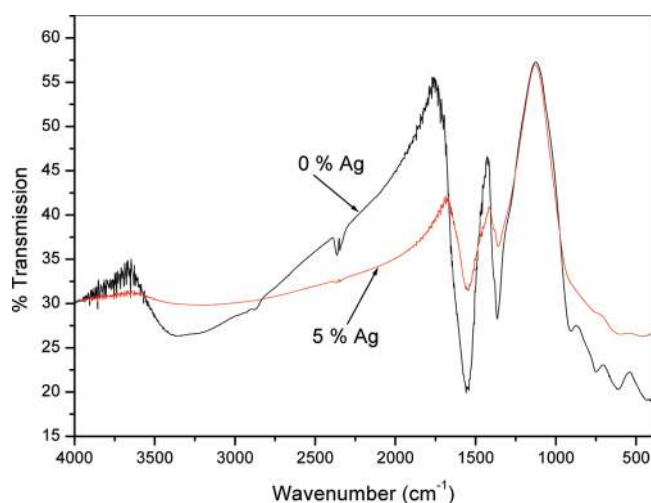


Figure 6. IR spectra of TiO₂ powders with different mol % silver content after aging at 100 °C for 12 h.

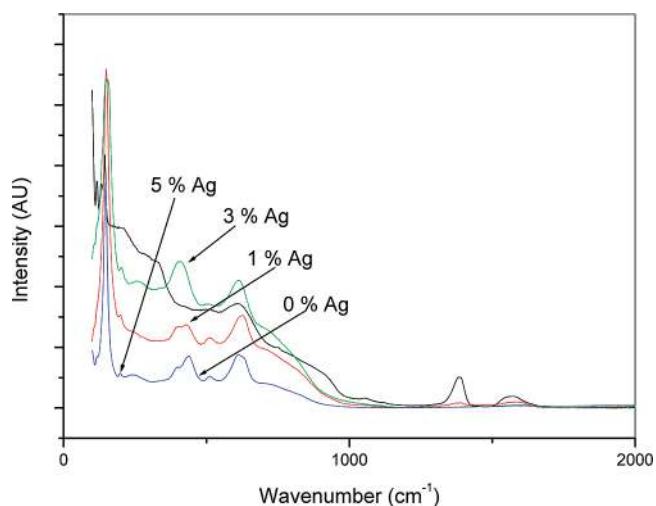


Figure 7. Raman spectra of TiO₂ powders with different mol % silver content before calcination.

241 also causes significant changes in the TiO region of the spectra
 242 (0–1000 cm⁻¹). The presence of peaks at 160, 420, 515, and
 243 620 in the Raman of the silver doped TiO₂ are indicative of the
 244 four peak pattern that would be expected for anatase.^{57–59}
 245 However, without the presence of silver, this four-peak pattern

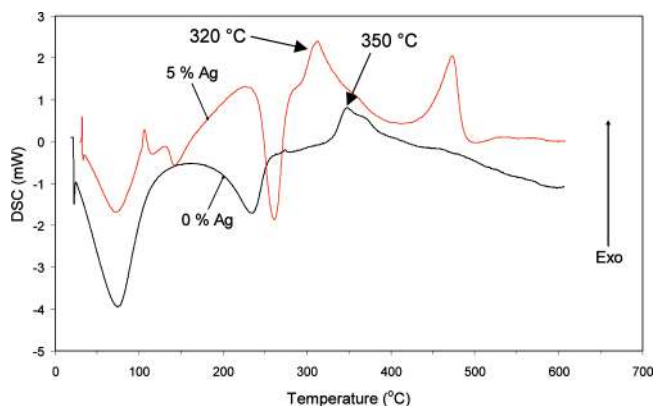


Figure 8. DSC of 0 and 5% Ag before aging.

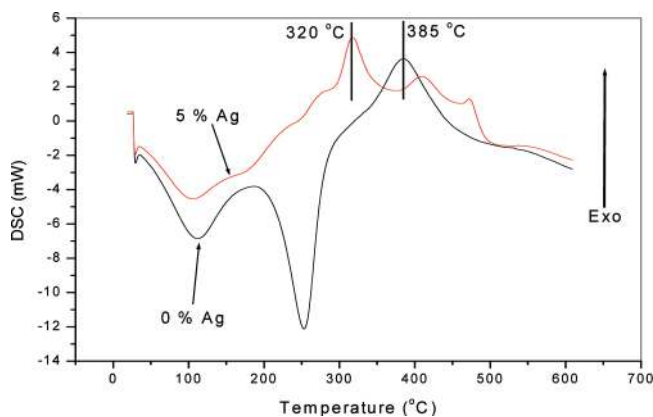


Figure 9. DSC of 0 and 5% Ag after aging at 100 °C.

is not as distinctive, again providing further evidence that silver
 effects the titanium formate complex before crystallization has
 occurred.

It is agreed that the use of a chelating agent gives stability to
 the hydrolysis and condensation reactions associated with the
 sol–gel process in the production of TiO₂ from titanium
 alkoxides.^{54,60–64} IR and Raman spectroscopy have shown that
 formic acid forms a bridging ligand with titania.^{55,65–68} Previous
 reports have shown that similar chelating agents remain bound
 to the central titanium atom, while the isopropoxy (OR) groups
 are preferentially hydrolyzed. The bridging ligands remain
 throughout much of the condensation process,^{54,56} altering the
 condensation pathway and promoting the formation of linear
 polymers composed of edge sharing octahedral.^{39,56} The system
 may be destabilized through the addition of water, which leads
 to a structurally weak network that can easily collapse upon
 calcination to form rutile.^{69,70}

From the spectroscopy results it can be seen that the addition
 of silver causes a reduction in the intensity of the COO⁻
 stretches indicating that the titania formate bridging complex
 is becoming weaker in the presence of silver. This may lead to
 a structurally weak oligomer that upon calcination easily forms
 rutile at lower temperatures.

DSC. DSC was carried out to investigate the thermal events
 associated with the doped and undoped TiO₂ samples before
 and after aging.

The DSC curve of the undoped TiO₂ powder analyzed before
 aging (Figure 8) is almost identical to the same sample after
 aging (Figure 9). It reveals an endothermic peak at ~100 °C
 attributed to the elimination of unbound water and formic acid
 from the surface of the TiO₂ powder. The same peak for the
 silver doped sample reveals as expected, a smaller enthalpy of

246
 247
 248
 249
 250
 251
 252
 253
 254
 255
 256
 257
 258
 259
 260
 261
 262
 263
 264
 265
 266
 267
 268
 269
 270
 271
 272
 273 F8
 274 F9
 275
 276
 277

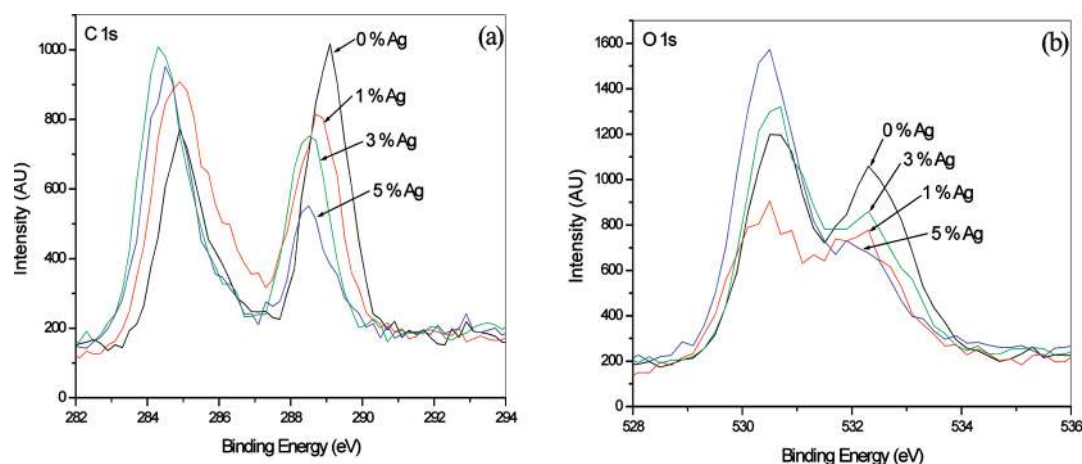


Figure 10. XPS spectra of C 1s (a) and O 1s (b) of TiO₂ with and without silver before calcination.

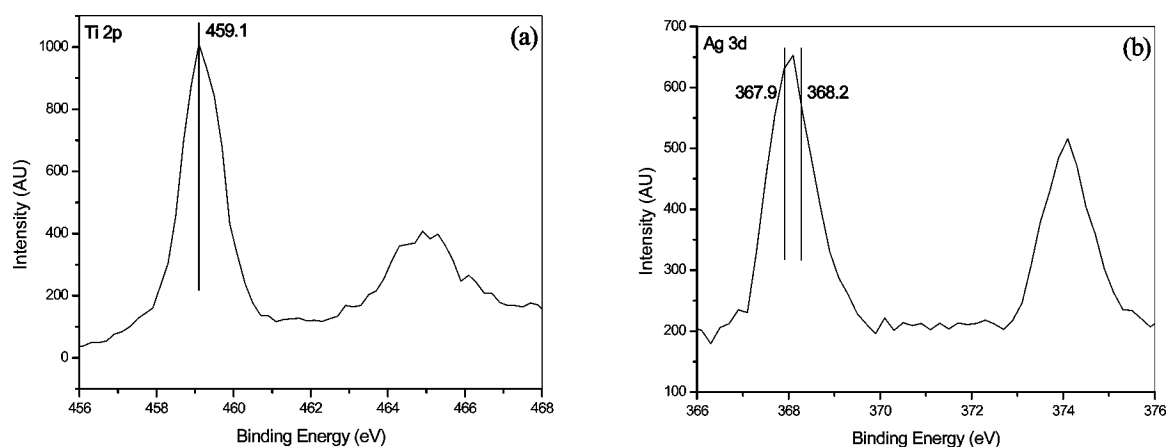


Figure 11. XPS spectra of Ti 2p (a) and Ag 3d (b) of 3% Ag TiO₂ before calcination.

278 -420 J/g compared with -636 J/g for the undoped sample,
 279 indicating that formic acid is easier to remove in the presence
 280 of silver. This is in agreement with the previously proposed
 281 mechanism from the FTIR and Raman spectroscopy results, that
 282 silver inhibits formic acid and it is thus removed upon aging at
 283 100 °C therefore, allowing the oligomer structure to readily
 284 collapse and form rutile upon calcination.

285 In Figures 8 and 9 an endothermic peak at ~ 250 °C is due
 286 to the removal of isopropanol formed through the condensation
 287 step. The removal of isopropanol indicates that the condensation
 288 step is complete. Comparing the DSC curves of the samples
 289 before (Figure 8) and after (Figure 9) aging shows that the
 290 endothermic isopropanol peak is present in both the 0 and 5
 291 mol % silver sample before aging. But after aging the isopro-
 292 panol peak at 250 °C is only present with 0% Ag TiO₂. This
 293 provides further explanation for the formation of rutile at lower
 294 temperatures, since when the condensation step is near comple-
 295 tion, the crystallization temperature is lowered and then so too
 296 is the anatase to rutile transformation temperature.

297 The appearance of the first exothermic peak in all DSC curves
 298 is the transition from amorphous TiO₂ to crystalline anatase,
 299 and as expected this peak occurs earlier with silver doped TiO₂
 300 than with TiO₂ only. Figure 8 shows that crystallization occurs
 301 at 320 °C for 5% Ag TiO₂ but does not occur until 350 °C for
 302 the undoped sample. This can also be seen in Figure 9 where
 303 crystallization of 5% Ag TiO₂ takes place at 320 °C but for the
 304 undoped sample crystallization does not occur until 385 °C.

305 **XPS.** To determine more information on exactly how the
 306 silver is interacting with the titanium formate complex, XPS
 307 was carried out on the silver doped and undoped samples before

calcination to establish the titanium structure, the chemical state
 of the silver particles, and also for further evidence of the
 reduction in the carboxylate species. XPS spectra were recorded
 of the samples precalcination (as with IR and Raman) and XPS
 was also carried out on the crystalline titania after calcination.
 The spectra of C1s and O1s of TiO₂ without silver show the
 presence of the carboxylate group at 289.1^{71} and 532.3 eV,^{71,72}
 respectively (parts a and b of Figure 10). As the silver content
 is increased the intensity of these peaks decreases in a similar
 manner as those of the IR and Raman results, again indicating
 that with increased silver content, the formation of a titania
 formate bridging complex becomes increasingly difficult to
 form.

Figure 11 shows the XPS narrow scans for Ti 2p and Ag 3d
 peaks. The XPS spectrum of Ti 2p is unchanged with increasing
 amounts of silver, the Ag 3d spectrum of 1% silver TiO₂ gives
 a weaker signal than the 3% shown in figure 11b and the Ag
 3d scan of 5% silver TiO₂ results in a spectrum similar to 3%
 silver TiO₂. The fact that increasing amounts of silver does not
 affect the Ti 2p spectra indicates that central titanium atom has
 not been reduced. In Figure 11a, a Ti 2p peak at 459.1 eV is
 representative of Ti in its tetravalent state⁷³ in an octahedral
 environment.⁷⁴ The absence of a Ti³⁺ peak at 457.4 eV leads
 to the following observations.

(1) Ti has not been reduced to Ti³⁺ which may indicate an
 absence of surface oxygen vacancies.⁷⁵ However, if TiO_{*n*} (*n* <
 2) is formed it may not be present in detectable amounts.⁷⁶

(2) Ag₂O or Ag⁰ incorporation into the TiO₂ lattice may give
 rise to a signal at 457.4 eV representative of Ti³⁺.³⁶ From the

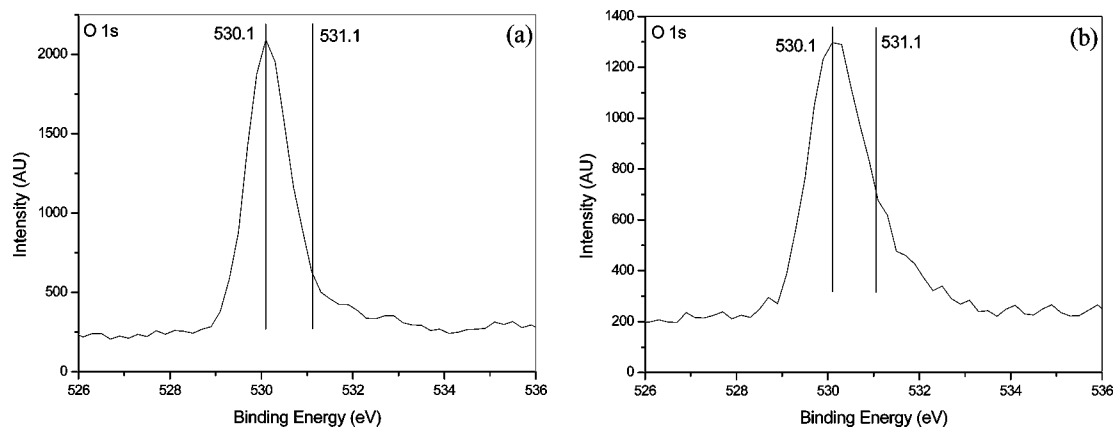


Figure 12. O 1s XPS spectra of TiO₂ without silver calcined at 900 °C (a) and with 3% silver calcined at 700 °C (b).

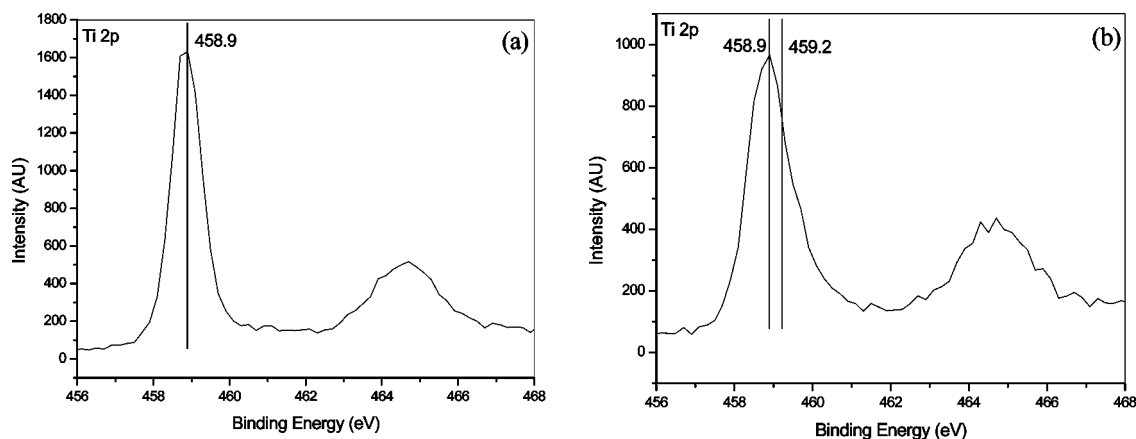


Figure 13. Ti 2p XPS spectra of TiO₂ without silver calcined at 900 °C (a) and with 3% silver calcined at 700 °C (b).

337 XPS there was no evidence of Ag TiO₂ bond formation, which
338 can be expected due to the differences in atomic radius.

339 The Ag 3d scan (Figure 11b) shows two large peaks. A
340 Gaussian fit of the main peak (~368 eV) showed that it was
341 made up of two signals at 367.9 and 368.2 eV, representing
342 the chemical bonding states of Ag₂O and Ag⁰, respectively.³⁶
343 Therefore, it has been shown that Ag⁰ and Ag₂O have formed
344 on the surface of the titania formate complex, before heat
345 treatment above 100 °C. Spectroscopic (FTIR, Raman, and XPS)
346 studies of the carbonyl species have shown a reduction in the
347 titanium formate bridging complex with increased amounts of
348 silver. The Ag 3d scan of a sample (before calcination)
349 containing silver (Figure 11b) shows the presence of Ag₂O
350 (Ag²⁺, 367.8 eV) and Ag⁰ (368.2 eV).³⁶ Therefore, the presence
351 of Ag₂O and Ag⁰ in the powders before calcination may be
352 responsible for the reduction of the titanium formate bridge as
353 shown by IR, Raman, and XPS. The presence of Ag₂O and Ag⁰
354 may then restrict the formation of a titanium formate bridging
355 complex which leads to an altered condensation pathway and
356 therefore low temperature formation of rutile.

357 Figure 12 shows the narrow scan XPS spectra for O 1s of
358 TiO₂ only calcined at 900 °C and 3% Ag TiO₂ calcined at 700
359 °C. Gaussian fits of both spectra give rise to two peaks at 530.1
360 and 531.1 eV for crystal lattice oxygen and hydroxy oxygen,
361 respectively.^{74,77} The silver doped sample contains a greater
362 amount of hydroxy oxygen. Chemisorbed surface hydroxyl
363 groups can enhance photocatalysis by trapping photoinduced
364 holes resulting in an increase in the formation of the highly
365 oxidizing OH[•] radicals.^{77,78} It is well reported that silver retards
366 the recombination of photogenerated electron hole pairs,^{36,37,79}
367 this may not only be due to the attraction of excited electrons

368 to silver but also due to the presence of extra hydroxyl species
369 to delay recombination through hole trapping.

370 There is an apparent difference between the Ti 2p spectra
371 shown in Figure 13. Unmodified TiO₂ gives a signal at 458.9
372 eV in the Ti 2p narrow scan. However, 3% silver TiO₂ results
373 in the presence of an additional signal at 459.2 eV. The undoped
374 sample after calcination at 900 °C gives a symmetrical peak at
375 458.9 eV (Figure 13a) typical of tetravalent Ti–O bond.⁷³
376 However, the Ti 2p narrow scan of the 3% Ag TiO₂ sample
377 calcined at 700 °C does not give a symmetrical peak. A Gaussian
378 fit of the spectrum gives two signals at 458.9 and 459.2 eV
379 both representing Ti–O,⁷³ but the shift in the binding energy
380 to 459.2 eV indicates that there may be an interaction between
381 TiO₂ and silver.⁸⁰

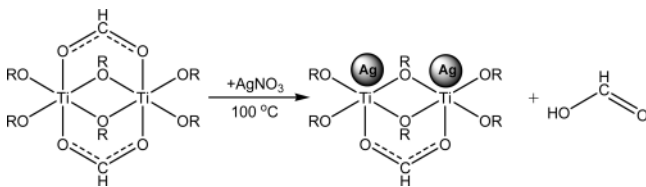
382 Through XPS, IR, and Raman it was shown that the addition
383 of silver restricts the formation of a titanium formate bridging
384 complex. XPS also shows that silver exists as both Ag⁰ and
385 Ag₂O. Finally, XPS has shown that the presence of silver results
386 in a peak being present at 459.2 eV in the Ti 2p scan (Figure
387 13b), which is indicative of an interaction between TiO₂ and
388 silver.⁸⁰ The combination of these results leads to the proposal
389 of Scheme 1. In Scheme 1 it is proposed that Ag⁰ and Ag₂O
390 block the formation of the titanium formate bridge. The resulting
391 titanium complex can then collapse readily upon calcination to
392 form rutile.

393 Gaussian fits of the narrow scan Ti 2p XPS spectra (Sup-
394 porting Information) of all samples before calcination reveals
395 two signals. The intensity of the signals accordingly varies with
396 the increasing presence of silver, further indicating that Ag⁰/
397 Ag₂O is interacting with titanium,⁸¹ thus facilitating the removal
398 of formate species and allowing for the collapse of the Ti–O

F13

S1

SCHEME 1: Illustration of Blocking Mechanism of Silver on the Titanium Formate Bridge



399 gel framework upon calcination to form rutile at lower
400 temperatures.

401 **Diffuse Reflectance Spectroscopy.** To estimate the band gap
402 distance, UV–vis spectroscopy was employed. The results show
403 that silver does improve visible light absorbance of TiO₂ due
404 to silver plasmon absorption; moreover, a blue shift was
405 observed for the band gap separation of the TiO₂ materials upon
406 increased silver addition.

F14 407 Figure 14 shows the diffuse reflectance spectra for 0, 1, 3,
408 and 5 mol % Ag TiO₂. It can be seen that unmodified TiO₂ has
409 a smaller band gap than the silver modified TiO₂. The blue shift
410 of the silver modified materials can be attributed to the presence
411 of additional silver.⁸²

F15 412 Figure 15 shows a diffuse reflectance spectrum of Ag
413 nanoparticles where a strong absorbance is observed at ~335
414 nm. The band gap of the TiO₂ nanomaterials can therefore not
415 be accurately determined because of the strong silver absorption.⁸³ It is also clear that the presence of increased amounts of
416 silver (3 and 5 mol %) facilitates visible light absorbance. This
417 can also be seen from Figure 15 through strong visible light
418 absorption of the silver nanoparticles. The proposed mechanism
419 for the visible light absorbance of Ag TiO₂ is shown in Figure
420 16.⁸⁰

F16 421
F17 422 It can also be seen in both Figures 14 and 17 that 3 mol %
423 silver TiO₂ has greater absorption than 5 mol % Ag in the visible
424 region. This is because increased levels of silver act as a physical
425 block against TiO₂ light absorption. This causes an increase in
426 the diffuse light reflectance of the material.³⁷

F18 427 In Figure 18 it is observed that the band gap of the modified
428 TiO₂ is reduced, as seen by the red shift in the spectra of the 3
429 and 5 mol % Ag TiO₂ in comparison with Figures 14 and 17.
430 This is attributed to the formation of rutile. Rutile has a smaller
431 band gap than anatase;¹³ XRD results confirm that silver doped
432 samples calcined at 800 °C have rutile structure (Figure 3). By

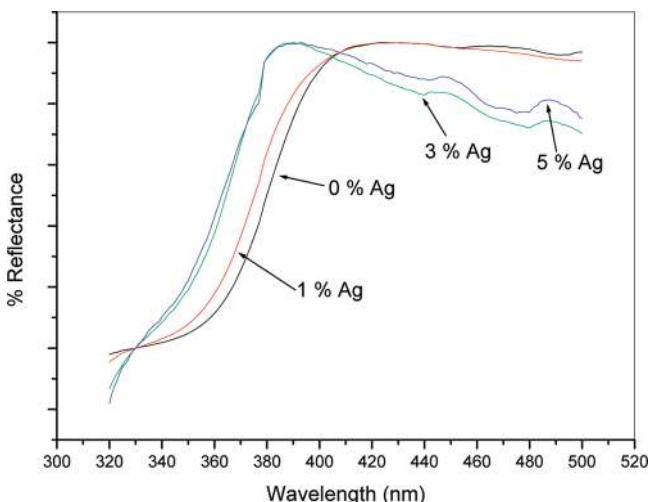


Figure 14. Diffuse reflectance spectra of 0, 1, 3, and 5% Ag TiO₂ calcined at 500 °C.

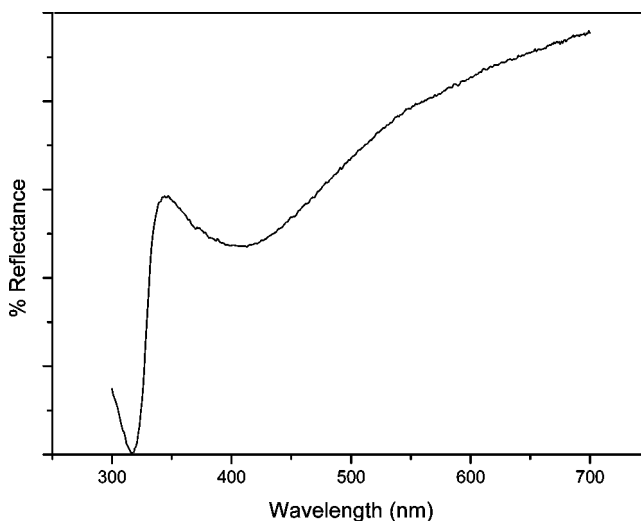


Figure 15. Diffuse reflectance spectrum of silver nanoparticles.

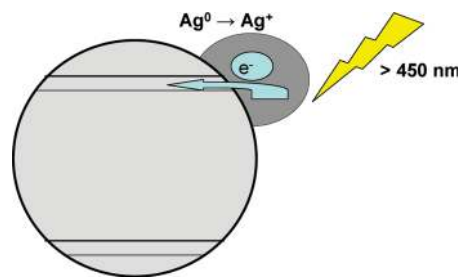


Figure 16. Mechanism for light absorption of silver.

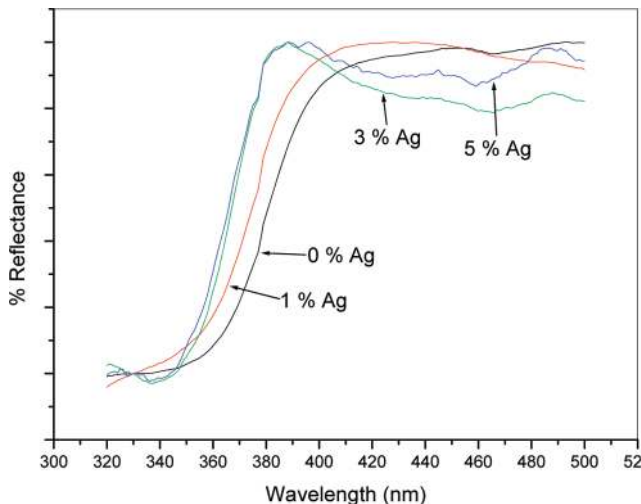


Figure 17. Diffuse reflectance spectra of 0, 1, 3, and 5% Ag TiO₂ calcined at 700 °C.

comparison of Figure 18 with Figures 14 and 17, silver does
not have the same influence in causing the blue shift. The
mechanism of anatase to rutile transformation is one of
nucleation and growth,^{46,47} therefore, rutile particles are
significantly larger than those of anatase. The larger particles may
result in a significant reduction in the influence of silver on the
band gap of the materials.

Conclusions

A systematic study of the effect of silver on the anatase to
rutile transformation temperature of TiO₂ has been carried out.
By use of XRD, FTIR, Raman, DSC, and XPS it was proposed
that the addition of silver blocks the formation of a titanium -

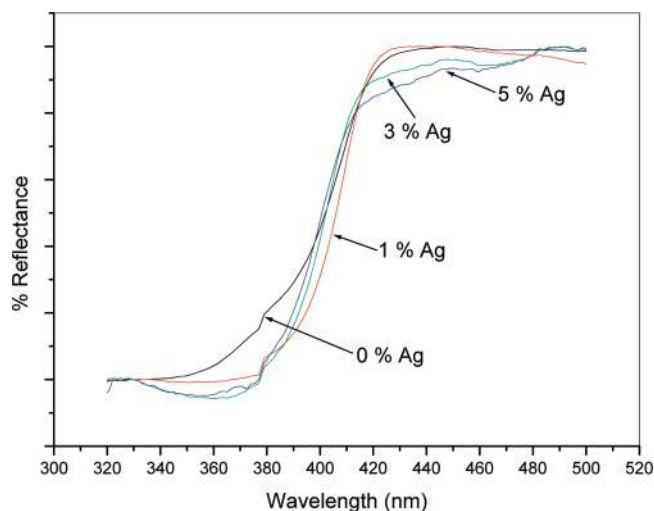


Figure 18. Diffuse reflectance spectra of 0, 1, 3, and 5% Ag TiO₂ calcined at 800 °C.

445 carboxylate bridging ligand. This was clearly shown through
 446 the carboxylate stretches in FTIR, Raman and XPS. Without
 447 the formation of this bridging ligand the condensation pathway
 448 is altered, and the resulting titania polymer network is weakened.
 449 When calcined, this weakened structure can readily transform
 450 from anatase to rutile due to a greater atomic mobility. The
 451 sample with no silver present maintained anatase at greater
 452 temperatures than those that contained silver. This was due to
 453 the formation of a strong carboxylate bridge that promoted a
 454 more organized structure throughout the condensation process.
 455 The more ordered oligomer network of the sample without silver
 456 consisted of anatase at greater temperatures than those where
 457 silver was present. This was clearly seen from the XRD
 458 diffractograms. Previous reports have indicated that oxygen
 459 vacancies contribute to the early formation of rutile, but through
 460 XPS and PL, it was concluded that the presence of additional
 461 silver did not form extra oxygen vacancies. XPS also showed
 462 that Ag₂O and Ag⁰ was present in the samples before high
 463 temperature calcination. It was also showed through XPS that
 464 there may be an interaction between Ag and Ti, which agrees
 465 with the proposed mechanism outlined in Scheme 1.

466 PL studies showed that the addition of silver reduced
 467 recombination of electron, hole pairs, and PL spectra did not
 468 provide any evidence for the presence of additional oxygen
 469 vacancies with increased amounts of silver. Diffuse reflectance
 470 showed greater visible light absorbance through silver plasmon
 471 resonance.

472 An alternative mechanism has been proposed on how silver
 473 effects the anatase to rutile transition of TiO₂. In the proposed
 474 mechanism, silver blocks the formation of a bridging ligand
 475 with the titanium alkoxide precursor. This is clearly shown in
 476 FTIR, Raman, and XPS spectra, and the resulting lower
 477 formation of rutile is clear from XRD and DSC.

478 **Acknowledgment.** The authors would like to thank the EPA
 479 for funding and DIT, focas, and CREST for materials and
 480 resources. The authors would also like to thank Aisling Kirwan
 481 for FESEM images. This paper is dedicated to Professor John
 482 M. Kelly, C. Chem. FRSC, on the occasion of completing 37
 483 years of teaching and research at Trinity College Dublin, Ireland.

484 **Supporting Information Available:** Figures depicting Ti
 485 2p XPS spectrum of 0, 1, 3, and 5% Ag before calcination and
 486 5 % silver loading on TiO₂ calcined at 700 and 800 °C. This

material is available free of charge via the Internet at <http://pubs.acs.org>. 487
488

References and Notes 489

- (1) Fox, M. A.; Dulay, M. T. *Chem. Rev.* **1993**, *93*, 341–357. 490
- (2) Hoffmann, M. R.; Martin, S. T.; Choi, W.; Bahnemann, D. W. *Chem. Rev.* **1995**, *95*, 69–96. 491
- (3) Honda, K.; Fujishima, A. *Nature* **1972**, *238*, 37. 492
- (4) Liu, H.; Cheng, S.; Wu, M.; Zhang, J.; Li, W.; Cao, C. *J. Phys. Chem. A* **2000**, *104*, 7016. 493
- (5) Tada, H.; Yamamoto, M.; Ito, S. *Langmuir* **1999**, *15*, 3699. 494
- (6) Xu, Y. M.; Langford, C. H. *Langmuir* **2001**, *17*, 897. 495
- (7) Yu, J.; Yu, H.; Ao, C. H.; Lee, S. C.; Yu, J. C.; Ho, W. *Thin Solid Films* **2006**, *496*, 273–280. 496
- (8) Yu, J. G.; Yu, H. G.; Cheng, B.; Zhao, X. J.; Yu, J. C.; Ho, W. K. *J. Phys. Chem. B* **2003**, *107*, 13871. 497
- (9) Yu, J. G.; Yu, J. G.; Ho, W. K.; Zhang, L. Z. *Chem. Commun.* **2001**, 1942. 498
- (10) Zhao, J.; Wu, T.; Wu, K.; Oikawa, K.; Hidaka, H.; Serpone, N. *Environ. Sci. Technol.* **1998**, *32*, 2394–2400. 499
- (11) Hu, Y.; Tsai, H.-L.; Huang, C.-L. *Eur. Ceram. Soc.* **2003**, *23*, 691–696. 500
- (12) Shao, Y.; Tang, D.; Sun, J.; Lee, Y.; Xiong, W. *China Particuology* **2004**, *2*, 119–123. 501
- (13) Carp, O.; Huisman, C. L.; Reller, A. *Prog. Solid State Chem.* **2004**, *32*, 33–177. 502
- (14) Aguado, J.; van Grieken, R.; Lopez-Munoz, M. J.; Marugan, J. *Catal. Today* **2002**, *75*, 95–102. 503
- (15) Diebold, U. *Surf. Sci. Reports* **2003**, *48*, 53–229. 504
- (16) Kuo, Y.-L.; Chen, H.-W.; Ku, Y. *Thin Solid Films* **2006**, *515*, 3461–3468. 505
- (17) Hamal, D. B.; Klabunde, K. J. *J. Colloid Interface Sci.* **2007**, *311*, 514–522. 506
- (18) Luo, H.; Takata, T.; Lee, Y.; Zhao, J.; Domen, K.; Yan, Y. *Chem. Mater.* **2004**, *16*, 846–849. 507
- (19) Asahi, R.; Morikawa, T.; Oikawa, K.; Aoki, K.; Taga, Y. *Science* **2001**, *293*, 269. 508
- (20) Ihara, T.; Miyoshi, M.; Iriyama, Y.; Matsumoto, O.; Sugihara, S. *Appl. Catal. B* **2003**, *42*, 403–409. 509
- (21) Martyanov, I. N.; Uma, S.; Rodrigues, S.; Klabunde, K. J. *Chem. Commun.* **2004**, 2476–2477. 510
- (22) Umebayashi, T.; Yamaki, T.; Itoh, H.; Asai, K. *Appl. Phys. Lett.* **2002**, *81*, 454–456. 511
- (23) Khan, S. U. M.; Al-Shahry, M.; Ingler, W. B. *Science* **2002**, *297*, 2243–2245. 512
- (24) Hong, X.; Wang, Z.; Cai, W.; Lu, F.; Zhang, J.; Yang, Y.; Ma, N.; Liu, Y. *Chem. Mater.* **2005**, *17*, 1548–1552. 513
- (25) Choi, W.; Termin, A.; Hoffmann, M. R. *J. Phys. Chem.* **1994**, *98*, 533. 514
- (26) Nagaveni, K.; Hegde, M. S.; Madras, G. *J. Phys. Chem. B* **2004**, *108*, 535. 515
- (27) Wang, W.; Zhang, J.; Chen, F.; He, D.; Anpo, M. *J. Colloid Interface Sci.* **2008**, *323*, 182–186. 516
- (28) Zhu, J.; Chen, F.; Zhang, J.; Chen, H.; Anpo, M. *J. Mol. Catal. A* **2004**, *216*, 537. 517
- (29) Zhu, J.; Deng, Z.; Chen, F.; Zhang, J.; Chen, H.; Anpo, M.; Huang, J.; Zhang, L. *Appl. Catal. B* **2006**, *62*, 538. 518
- (30) Demeestre, K.; Dewulf, J.; Ohno, T.; Salgado, P. H.; Langenhove, H. V. *Appl. Catal. B* **2005**, *61*, 140. 519
- (31) Behar, D.; Rabani, J. *J. Phys. Chem. B* **2006**, *110*, 8750. 520
- (32) Kim, S. K.; Hwang, S. J.; Choi, W. *Sci. Technol.* **2005**, *35*, 2381. 521
- (33) Li, X. Z.; Li, F. B. *Environ. Sci. Technol.* **2001**, *35*, 2381. 522
- (34) You, X.; Chen, F.; Zhang, J.; Anpo, M. *Catal. Lett.* **2005**, *102*, 247. 523
- (35) Chao, H. E.; Yun, Y. U.; Xingfang, H. U.; Larbot, A. *ECERS* **2003**, *23*, 1457–1464. 524
- (36) Kuo, Y.-L.; Chen, H.-W.; Ku, Y. *Thin Solid Films* **2007**, *515*, 3461–3468. 525
- (37) Seery, M. K.; George, R.; Floris, P.; Pillai, S. C. *J. Photochem. Photobiol. A* **2007**, *189*, 258–263. 526
- (38) Choi, H.; Stathatos, E.; Dionysiou, D. D. *Top. Catal.* **2007**, *44*, 513–521. 527
- (39) Livage, J.; Sanchez, C.; Henry, M.; Doeuff, S. *Solid State Ionics* **1989**, *32/33*, 633–638. 528
- (40) Nolan, N. T.; Seery, M. K.; Pillai, S. C. *J. Phys. Chem. C* **2009**, *113*, 16151–16157. 529
- (41) Pillai, S. C.; Periyat, P.; George, R.; McCormack, D. E.; Seery, M. K.; Hayden, H.; Colreavy, J.; Corr, D.; Hinder, S. J. *J. Phys. Chem. C* **2007**, *111*, 1605–1611. 530
- (42) Periyat, P.; Pillai, S. C.; McCormack, D. E.; Colreavy, J.; Hinder, S. J. *J. Phys. Chem. C* **2008**, *112*, 7644–7652. 531
- (43) Periyat, P.; McCormack, D. E.; Hinder, S. J.; Pillai, S. C. *J. Phys. Chem. C* **2009**, *113*, 3246–3253. 532

- 568 (44) Spurr, R.; Myers, H. *Anal. Chem.* **1957**, *29*, 760.
 569 (45) Oliveri, G.; Ramis, G.; Busca, G.; Sanchez Escribano, V. *J. Mater.*
 570 *Chem.* **1993**, *3*, 1239–1249.
 571 (46) Ding, X.-Z.; Liu, X.-H. *J. Mater. Res.* **1998**, *13*, 2556–2559.
 572 (47) Gribb, A. A.; Banfield, J. F. *Am. Mineral.* **1977**, *82*, 717–728.
 573 (48) Zhang, H.; Banfield, J. F. *J. Mater. Res.* **2000**, *15*, 437–448.
 574 (49) Ahn, Y. U.; Kim, E. J.; Kim, H. T.; Hahn, S. H. *Mater. Lett.* **2003**,
 575 *57*, 4660–4666.
 576 (50) Hishita, S.; Mutoh, I.; Koumoto, K.; Yanagida, H. *Ceram. Intern.*
 577 **1982**, *9*, 61–67.
 578 (51) MacKenzie, K. J. D. *J. Brit. Ceram. Soc.* **1975**, *74*, 77–84.
 579 (52) Epifani, M.; Giannini, C.; Tapfer, L.; Vasanelli, L. *J. Am. Ceram.*
 580 *Soc.* **2000**, *85*, 2385–2393.
 581 (53) Litter, M. I. *Appl. Catal. B* **1999**, *23*, 89–114.
 582 (54) Brinker, C. J.; Scherer, G. W. *The Physics and Chemistry of Sol–*
 583 *Gel Science*; Academic Press: New York, 1990.
 584 (55) Nakamoto, K. *Infrared and Raman Spectra of Inorganic and*
 585 *Coordinated Compounds*; John Wiley: New York, 1997.
 586 (56) Nguyen, T.-V.; Choi, D.-J.; Yang, O.-B. *Res. Chem. Intermed.* **2005**,
 587 *31*, 483–491.
 588 (57) Hwang, D. S.; Lee, N. H.; Lee, D. Y.; Song, J. S.; Shin, S. H.;
 589 Kim, S. J. *Smart Mat. Struct.* **2006**, *15*, S74–S80.
 590 (58) Kittaka, S.; K., M.; Takahara, S. *J. Solid State Chem.* **1997**, *132*,
 591 447–450.
 592 (59) Yoshitake, H.; Abe, D. *Microporous Mesoporous Mater.* **2009**, *119*,
 593 267–275.
 594 (60) Guilment, J.; Pencilot, O.; Rigola, J.; Truchet, S. *Vib. Spectrosc.*
 595 **1996**, *11*, 37–49.
 596 (61) Phule, P. P.; Risbud, S. H. *J. Mater. Sci.* **1990**, *25*, 1169–1183.
 597 (62) Sanchez, C.; Livage, J.; Henry, M.; Babonneau, F. *J. Non-Cryst.*
 598 *Solids* **1988**, *100*, 65–76.
 599 (63) Takahaschi, Y.; Kiwa, K.; Kobayashi, K.; Matsuki, M. *J. Am.*
 600 *Ceram. Soc.* **1991**, *74*, 67–71.
 601 (64) Takahaschi, Y.; Matsuoka, Y. *J. Mater. Sci.* **1988**, *23*, 2259–2266.
 602 (65) Czakis-Sulikowska, D.; Czynkowska, A.; Malinowska, A. *J. Therm.*
 603 *Anal. Cal.* **2002**, *67*, 667–668.
 (66) Deacon, G. B.; Phillip, R. J. *Coord. Chem. Rev.* **1980**, *33*, 227– 604
 250. 605
 (67) Lewandowski, W.; Fuks, L.; Lewandowski, H. *J. Inorg. Biochem.* 606
2005, *99*, 1407–1423. 607
 (68) Manhas, B. S.; Trikha, A. K. *J. Indian Chem. Soc.* **1982**, *59*, 315– 608
 319. 609
 (69) Kung, H. H.; Ko, E. I. *Chem. Eng. J.* **1996**, *64*, 203–214. 610
 (70) Suresh, C.; Biju, V.; Mukundan, P.; Warriar, K. G. K. *Polyhedron* 611
1998, *17*, 3131–3135. 612
 (71) Ben Amor, S.; Baud, G.; Jacquet, M.; Nanse, G.; Fioux, P.; Nardin, 613
 M. *Appl. Surf. Sci.* **2000**, *153*, 172–183. 614
 (72) Korosi, L.; Papp, S.; Menesi, J.; Illes, E.; Zollmer, V.; Richardt, 615
 A.; Dekany, I. *Colloids Surf. A* **2008**, *319*, 136–142. 616
 (73) Xu, W.-X.; Zhu, S.; Fu, X.-C. *Appl. Surf. Sci.* **1998**, *136*, 194– 617
 205. 618
 (74) Barlier, V.; Bounor-Legare, V.; Boiteux, G.; Davenas, J.; Leonard, 619
 D. *Appl. Surf. Sci.* **2008**, *254*, 5408–5412. 620
 (75) Henderson, M. A. *Surf. Sci.* **1999**, *419*, 174–187. 621
 (76) Hoflund, G. F.; Yin, H. L.; Grogan, A. L., Jr.; Asbury, D. A. 622
Langmuir **1988**, *4*, 346–350. 623
 (77) Xu, J.; Chang, Y.; Zhang, Y.; Ma, S.; Qu, Y.; Xu, C. *Appl. Surf.* 624
Sci. **2008**, *255*, 1996–1999. 625
 (78) Akyol, A.; Yatmaz, H. C.; Bayramoglu, M. *Appl. Catal. B* **2004**, 626
54, 19–24. 627
 (79) Liqiang, J.; Yichun, Q.; Baiqi, W.; Shudan, L.; Baojiang, J.; Libin, 628
 Y.; Wei, F.; Honggang, F.; Jiazhong, S. *Solar Energy Mater. Solar Cells* 629
2006, *90*, 1773–1787. 630
 (80) Gunawan, C.; Teoh, W. Y.; Marquis, C. P.; Lifia, J.; Amal, R. *Small* 631
2009, *5*, 341–344. 632
 (81) Spojakina, A.; Krалеva, E.; Jiratova, K.; Petrov, L. *Appl. Catal. A* 633
2005, *288*, 10–17. 634
 (82) He, C.; Xiong, Y.; Chen, J.; Zha, C.; Zhu, X. *J. Photochem.* 635
Photobiol. A **2003**, *157*, 71–79. 636
 (83) Sen, S.; Mahanty, S.; Roy, S.; Heintz, O.; Bourgeois, S.; Chaumont, 637
 D. *Thin Solid Films* **2005**, *474*, 245–249. 638
 JP1016054 639